Human Molecular Genetics, 2015, Vol. 24, No. 12 3322–3334

doi: 10.1093/hmg/ddv082
Advance Access Publication Date: 3 March 2015
Original Article

ORIGINAL ARTICLE

Mutated myocilin and heterozygous Sod2 deficiency act synergistically in a mouse model of open-angle glaucoma

Myung Kuk Joe[1], Naoki Nakaya[1], Mones Abu-Asab[2] and Stanislav I. Tomarev[1,*]

[1]Section on Retinal Ganglion Cell Biology, Laboratory of Retinal Cell and Molecular Biology and [2]Histology Core, National Eye Institute, NIH, Bethesda, MD 20895, USA

*To whom correspondence should be addressed at: Building 6, Room 212, 6 Center Drive, SRGCB, LRCMB, National Eye Institute, NIH, Bethesda, MD 20892, USA. Tel: +1 301 4968524; Fax: +1 301 4802610; Email: tomarevs@nei.nih.gov

Abstract

Glaucoma is a multifactorial optic neuropathy characterized by retinal ganglion cell (RGC) death and axonal degeneration leading to irreversible blindness. Mutations in the *MYOCILIN* (*MYOC*) gene are the most common genetic factors of primary open-angle glaucoma. To develop a genetic mouse model induced by the synergistic interaction of mutated myocilin and another significant risk factor, oxidative stress, we produced double-mutant mice (Tg-MYOC$^{Y437H/+}$/Sod2$^{+/-}$) bearing human *MYOC* with a Y437H point mutation and a heterozygous deletion of the gene for the primary antioxidant enzyme, superoxide dismutase 2 (SOD2). Sod2 is broadly expressed in most tissues including the trabecular meshwork (TM) and heterozygous *Sod2* knockout mice exhibit the reduced SOD2 activity and oxidative stress in all studied tissues. Accumulation of Y437H myocilin in the TM induced endoplasmic reticulum stress and led to a 45% loss of smooth muscle alpha-actin positive cells in the eye drainage structure of 10- to 12-month-old Tg-MYOC$^{Y437H/+}$/Sod2$^{+/-}$ mice as compared with wild-type littermates. Tg-MYOC$^{Y437H/+}$/Sod2$^{+/-}$ mice had higher intraocular pressure, lost about 37% of RGCs in the peripheral retina, and exhibited axonal degeneration in the retina and optic nerve as compared with their wild-type littermates. Single-mutant littermates containing MYOC$^{Y437H/+}$ or Sod2$^{+/-}$ exhibited no significant pathological changes until 12 months of age. Additionally, we observed elevated expression of endothelial leukocyte adhesion molecule-1, a human glaucoma marker, in the TM of Tg-MYOC$^{Y437H/+}$/Sod2$^{+/-}$ mice. This is the first reported animal glaucoma model that combines expression of a glaucoma-causing mutant gene and an additional mutation mimicking a deleterious environment factor that acts synergistically.

Introduction

Glaucoma is a progressive optic neuropathy characterized by retinal ganglion cell (RGC) death, degeneration of axons in the optic nerve, and specific deformation of the optic nerve head (ONH) known as glaucomatous cupping (1). Primary open-angle glaucoma (POAG) is the most common form of glaucoma, with elevated intraocular pressure (IOP) being one of the main risk factors (2). Globally, more than 70 million people suffer from glaucoma, rendering it the second leading cause of blindness in the world. Since glaucoma prevalence increases with age, the number of glaucoma patients is expected to increase as the human life span continues to lengthen (1,3). Despite the high prevalence and severity of glaucoma, the biological basis of glaucoma is poorly understood and the factors contributing to its progression have not yet been fully elucidated.

The contribution of genetic variations to the development of POAG has been proven and disease-associated genes identified (4,5). Among them, the first identified and most commonly studied gene is *MYOCILIN* (*MYOC*), which encodes a glycoprotein consisting of 504 amino acids in humans. Mutations in *MYOC* are

Received: December 22, 2014. **Revised:** February 13, 2015. **Accepted:** March 2, 2015

responsible for approximately 3–5% of adult-onset POAG and 10–30% of juvenile-onset open-angle glaucoma (5–7). So far, more than 70 different glaucoma-associated mutations have been identified in *MYOC*, and the majority of these mutations are within the third exon of the gene encoding the olfactomedin domain at the carboxyl terminus of the protein (8,9). Disease-causing mutant myocilins are non-secreted (10), relatively insoluble (11), form intracellular aggregates containing amyloid fibrils (12), and are accumulated in ER as aggregates leading to ER stress, which ultimately may lead to cell death (13–17). Myocilin is abundantly expressed in the trabecular meshwork (TM), one of the key components of the eye's aqueous humor outflow system (18,19). This suggests that accumulation of mutated myocilin in TM could lead to ER stress, and ultimately may result in the loss of cells within the TM, structural changes in the outflow pathway, and elevated IOP (16,17). Several transgenic mouse lines expressing mutated mouse or human myocilin in the TM have been generated to produce a mouse glaucoma model, allowing a better understanding of the *in vivo* pathogenic mechanisms induced by mutated myocilin (20–23). We have generated transgenic mice using a bacterial artificial chromosome containing the full-length human *MYOC* gene with the Y437H point mutation. These mice produced physiological levels of mutated Y437H human myocilin in the iridocorneal angle tissues (20). The expressed mutant myocilin accumulated in the TM and led to up-regulation of ER stress markers and down-regulation of paraoxonase 2 and glutathione peroxidase 3 in the eye angle tissues of aged (16-month-old) transgenic mice that help to defend against oxidative stress (16). However, moderate IOP elevation and loss of RGCs in the peripheral retina were detected only in aged (16- to 18-month-old) mice. Expression of the same human Y437H mutant myocilin at much higher level in the TM of transgenic mice using the CMV promoter led to more dramatic elevation of IOP and RGC loss that could be detected even in 3- to 5-month-old mice (23).

Available data suggest that interactions between genetic and environmental factors confer the complex disease phenotypes of POAG (24–27). This implies that individuals carrying POAG-associated genetic variants of certain genes may be more susceptible to the development of the disease when they are exposed to particular environmental factors. Environmental factors and unhealthy lifestyles—like atmospheric pollutants, cigarette smoke, ultraviolet rays, radiation, and toxic chemicals—can create an imbalance between pro-oxidants and antioxidants, leading to oxidative stress (28). Oxidative and ER stress are intimately interconnected (29). It has been shown that expression of mutated myocilin in primary TM cultures impairs mitochondrial functions (30), while expression of mutated myocilin in HEK293 cells make them more sensitive to oxidative stress (16). This led to a suggestion that TM of people carrying mutations in *MYOC* might be more sensitive to the oxidative stress produced by environmental factors.

Here, to test this hypothesis in an animal model, we applied oxidative stress to our transgenic mouse line that expresses the human Y437H myocilin mutant by mating this line with mice carrying a null mutation of *Sod2* (superoxide dismutase 2). SOD2, a critical enzyme for aerobic life (31), is a detoxification enzyme that converts superoxide to hydrogen peroxide, which can subsequently be converted to water. SOD2 is broadly expressed in most tissues including human TM cells and rat eye angle tissues (32,33). The homozygous *Sod2* knockout mice survive only for a short time (34). However, heterozygous *Sod2* knockout mice exhibit an apparently normal phenotype and life span, despite the reduced activities of the enzyme and excessive oxidative stress in all studied tissues (35). We report that mice that express human mutated myocilin in the TM and are heretozygous for the *Sod2* null mutation develop more severe glaucoma-like phenotype much earlier than mice carrying just myocilin mutation. Pathogenic mechanisms activated in this double-mutant mouse model may better reflect the pathology observed in human patients carrying mutations in *MYOC*.

Results

Mutated myocilin and *Sod2* haplodeficiency together induce elevated levels of apoptotic and ER stress markers *in vivo*

Since expression of mutated myocilin makes cells in culture more sensitive to oxidative stress, we hypothesized that *in vivo* expression of mutated myocilin in transgenic mice would similarly increase the sensitivity of TM cells to oxidative stress and promote cell death (16). To apply additional oxidative stress to the TM, we mated MYOC$^{Y437H/+}$ transgenic mice with *Sod2*-deficient mice, producing double-mutant Tg-MYOC$^{Y437H/+}$/Sod2$^{+/-}$ mice. Heterozygous *Sod2* knockout mice provide higher levels of oxidative stress to TM, since *Sod2* is expressed in most types of cells and tissues including TM cells and heterozygous null mice exhibit excessive oxidative stress in all studied tissues (32,36,37). We have previously detected up-regulation of an ER stress marker, 78 kDa glucose-regulated protein (GRP78), in the angle tissues of 16-month-old Tg-MYOC^{Y437H} mice (16). To test whether induction of ER stress occurs earlier in Tg-MYOC$^{Y437H/+}$/Sod2$^{+/-}$ mice, we compared the levels of GRP78 in the angle tissues of Tg-MYOC$^{Y437H/+}$/Sod2$^{+/-}$, Tg-MYOC$^{Y437H/+}$, Sod2$^{+/-}$, and wild-type mice from 4-month-old onward. No changes in the level of GRP78 were detected in the angle tissues among 4- to 6-month-old mice of different genotypes. Similarly, no changes were detected in the level of apoptotic marker, cleaved poly (ADP-ribose) polymerase (PARP), in mice of this age (not shown). However, the level of GRP78 was increased in 8-month-old Tg-MYOC$^{Y437H/+}$/Sod2$^{+/-}$ mice as compared with other genotypes (Fig. 1A and B). To test whether induction of ER stress in MYOC$^{Y437H/+}$/Sod2$^{+/-}$ mice is accompanied by the induction of apoptosis, we selected two apoptotic markers. Bcl-2 interacting mediator of cell death (Bim), a pro-apoptotic BH3-only member of the Bcl-2 family, is required for the initiation of apoptosis induced by severe ER stress (38). Cleaved PARP is generated by activated caspases 3 and 7 during apoptosis and is considered a major hallmark of apoptosis (39). Bim and cleaved PARP were increased in the angle tissues of 8-month-old Tg-MYOC$^{Y437H/+}$/Sod2$^{+/-}$ mice compared with other genotypes (Fig. 1A and B). Bright-field images revealed that the iridocorneal angle of Tg-MYOC$^{Y437H/+}$/Sod2$^{+/-}$ mice was open and had no obvious abnormalities in the structure of the iris, ciliary body, or cornea (Fig. 1C, upper panel). Immunostaining of eye sections with antibodies against GRP78 demonstrated elevated levels of staining in the TM and sclera of 8-month-old Tg-MYOC$^{Y437H/+}$/Sod2$^{+/-}$ mice and weak staining in Tg-MYOC$^{Y437H/+}$ mice, while wild-type and Sod$^{+/-}$ sections showed practically no staining (Fig. 1C, lower panel). These data confirmed our suggestion that a combination of elevated levels of reactive oxygen species (ROS) as a result of Sod2 haplodeficiency and mutated myocilin indeed produce more severe ER stress *in vivo* than either factor alone.

Mutated myocilin and *Sod2* haplodeficiency together decrease the number of cells and actin cytoskeleton in TM, and elevate IOP

Up-regulation of apoptotic markers in the eye angle tissues of Tg-MYOC$^{Y437H/+}$/Sod2$^{+/-}$ mice, as detected by Western blotting,

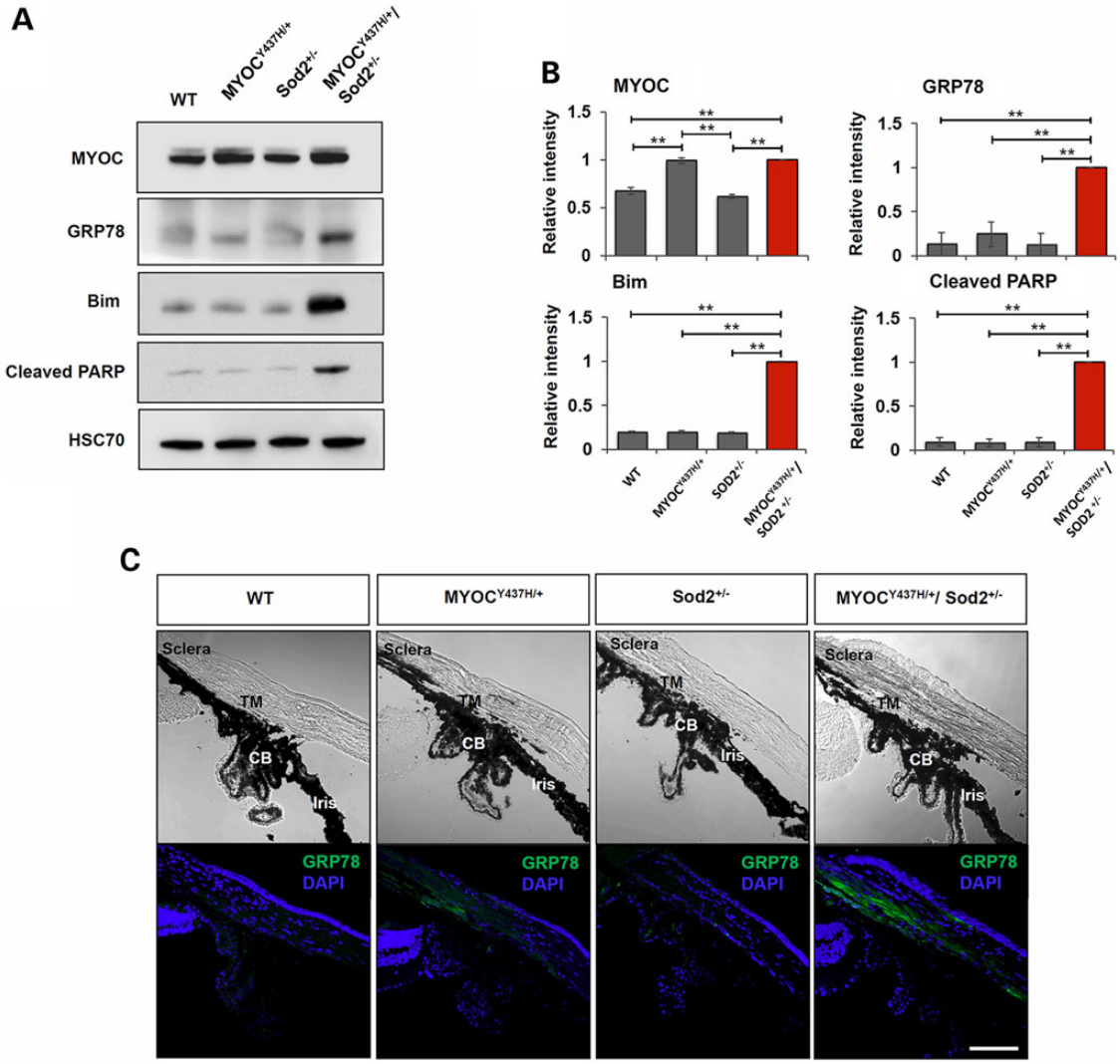

Figure 1. Increased expression of markers for ER stress and apoptosis in the eye angle tissue of Tg-MYOC$^{Y437H/+}$/Sod2$^{+/-}$ mice. (**A**) Lysates from the dissected eye angle tissues of 8-month-old littermates were immunoblotted with indicated antibodies. HSC70 was used as an internal control. (**B**) Quantification of three independent Western blot experiments as in (A). Signal intensities of all proteins analyzed were calculated relatively MYOC$^{Y437H/+}$/Sod2$^{+/-}$ samples, since the level of GRP78 was very low in some wild-type samples. $^{**}P < 0.01$. (**C**) Frozen eye sections of 8-month-old littermates were stained with antibodies against GRP78 and DAPI (lower panel). Upper panel shows the bright-field images. Eye sections from at least three independent mice of each genotype were used for staining. Representative images are shown. Scale bar, 100 μm; TM, trabecular meshwork; CB, ciliary body.

suggests apoptotic cell death and TM damage. To evaluate TM damage *in vivo*, we stained TM with antibodies against alpha-smooth muscle actin (α-SMA). In the eye, α-SMA expression was detected in the human aqueous outflow pathway (40). Staining of the eye sections of wild-type mice with antibodies against α-SMA demonstrated specific staining of the junction of the cornea and iris corresponding to the TM area (Fig. 2A). α-SMA staining was co-localized with myocilin staining in the TM, though myocilin staining extended further into the sclera (Fig. 2A). Staining of the whole mouse eye ball with antibodies against α-SMA showed a very specific signal, located at the expected TM position, and extended around the whole eye (Fig. 2B). For more careful examination of α-SMA staining, tissues around the TM were dissected (see a yellow square in Fig. 2B) and the staining patterns were compared between different genotypes. Strong α-SMA staining was observed in the TM area of wild-type mice (Fig. 2C). However, α-SMA signals were significantly reduced in the TM area of Tg-MYOC$^{Y437H/+}$/Sod2$^{+/-}$ mice and moderately reduced in Tg-MYOC$^{Y437H/+}$ mice when compared to wild-type and Sod2$^{+/-}$ mice (Fig. 2C). To estimate the number of cells in the TM, we stained nuclei with TO-PRO-3 and counted them in the α-SMA stained area. A significant loss of cells was detected in the TM of Tg-MYOC$^{Y437H/+}$/Sod2$^{+/-}$ mice as compared with other genotypes (Fig. 2D). The number of cells was reduced by 45% in 10- to 12-month-old Tg-MYOC$^{Y437H/+}$/Sod2$^{+/-}$ mice versus wild-type mice. There was a trend for a reduction of the cell number in Tg-MYOC$^{Y437H/+}$ mice that did not reach statistical significance (Fig. 2D). We suggest that expression of mutated myocilin and increased oxidative stress in Tg-MYOC$^{Y437H/+}$/Sod2$^{+/-}$ mice leads to TM cell loss and actin fiber reduction.

Available data suggest that loss of TM cells may lead to IOP elevation and be associated with glaucoma in humans (41). To test the effects of cell loss in the TM area of mice, we measured IOP in wild-type, Tg-MYOC$^{Y437H/+}$, Sod2$^{+/-}$, and Tg-MYOC$^{Y437H/+}$/Sod2$^{+/-}$ mice. Our previous data (20) and data of literature (42) demonstrated that there are no statistically significant IOP changes in

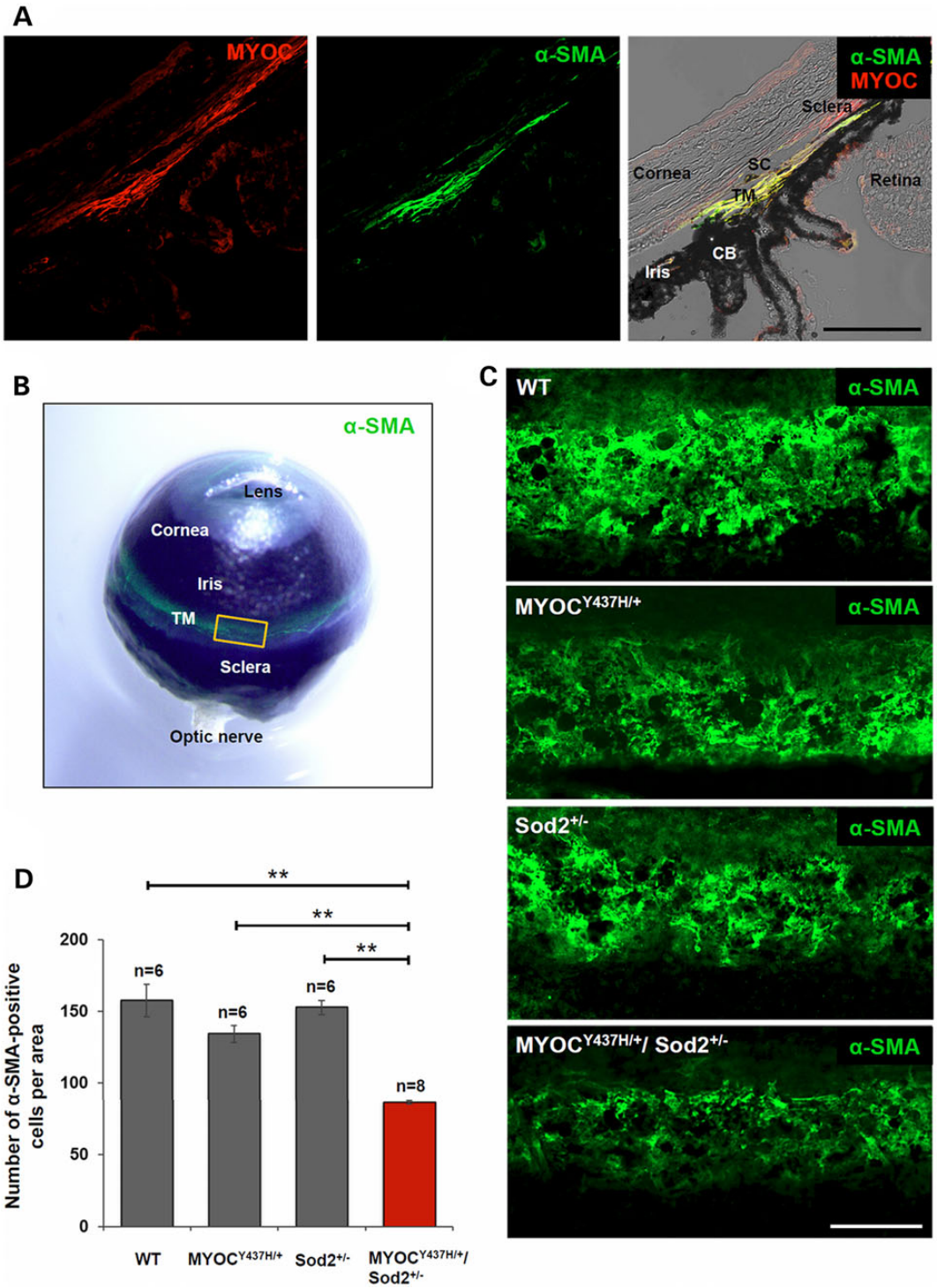

Figure 2. Reduction of α-SMA fibers and cells in TM of Tg-MYOC$^{Y437H/+}$/Sod2$^{+/-}$ mice. (**A**) Frozen eye sections of wild-type mice were stained with anti-myocilin (left panel) and anti-α-SMA (middle panel) antibodies. Right panel is the merged image of two fluorescent channels and bright field. Scale bar, 100 μm. (**B**) Whole mouse eye ball was stained with anti-α-SMA antibody and its green fluorescent image was overlaid on the bright-field image. The yellow square indicates a representative region encompassing TM shown in (**C**). (**C**) The anterior segments including TM were dissected from 10-month-old littermates and TM tissues in the segments were stained with α-SMA antibodies. At least six independent samples per each genotype were stained. Representative images are shown. Scale bar, 100 μm. (**D**) The nuclei in the α-SMA-positive area of 10- to 12-month-old mice were counted and represented as the numbers per region. All the values are presented as mean ± SE and analyzed by one-way ANOVA followed by Tukey's multiple comparisons test. $^{**}P < 0.01$. *n* shows the number of analyzed mice; TM, trabecular meshwork; CB, ciliary body; SC, Schlemm's canal.

Tg-MYOC$^{Y437H/+}$ or wild-type mice between 8 and 12 months of age. Tg-MYOC$^{Y437H/+}$/Sod2$^{+/-}$ mice also did not show statistically significant changes in IOP between 8- to 10- and 10-to 12-month-old age groups tested (now shown) and data for both groups were combined in Figure 3. Statistically significant elevation of IOP was detected in 8- to 12-month-old Tg-MYOC$^{Y437H/+}$/Sod2$^{+/-}$ mice

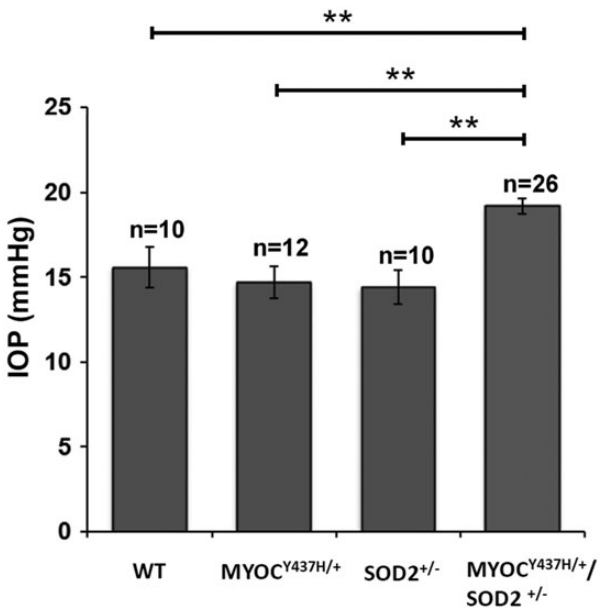

Figure 3. IOP elevation in the eyes of Tg-MYOC$^{Y437H/+}$/Sod2$^{+/-}$ mice. Results of IOP measurements in the eyes of 8- to 12-month-old mice are shown. All the values are presented as mean ± SE and analyzed by one-way ANOVA followed by Tukey's multiple comparisons test. **$P < 0.01$. *n* shows the number of analyzed mice.

relative to other mouse lines. There were no significant differences between wild-type and the two single-mutant mouse lines. The difference between Tg-MYOC$^{Y437H/+}$/Sod2$^{+/-}$ mice and mice from other genotypes ranged from 3.7 to 4.2 mmHg (Fig. 3). The elevation of IOP in Tg-MYOC$^{Y437H/+}$/Sod2$^{+/-}$ mice was almost 2-fold higher and was detected much earlier than in Tg-MYOC$^{Y437H/+}$ mice which we had analyzed previously (20).

RGC and axonal degeneration in Tg-MYOC$^{Y437H/+}$/Sod2 $^{+/-}$ mice

To characterize potential pathological changes in the retina of mice with different genotypes, we stained whole-mounted retinas with antibodies against markers of nerve fibers and RGCs. The retinal nerve fibers of 10-month-old mice were visualized by the staining with antibodies against neurofilament heavy chain protein (NFH). Overall, staining of the nerve fibers in peripheral retina of Tg-MYOC$^{Y437H/+}$/Sod2$^{+/-}$ mice was dramatically reduced, while staining of Sod2$^{+/-}$ retinas was moderately reduced, when compared with staining of wild-type and Tg-MYOC$^{Y437H/+}$ retinas but the reduction of staining in Sod2$^{+/-}$ retinas was not statistically significant ($P < 0.075$) (Fig. 4A and B). The temporal and ventral parts of Tg-MYOC$^{Y437H/+}$/Sod2$^{+/-}$ retina showed more pronounced reduction of staining than the dorsal and nasal parts (Fig. 4A). Less pronounced differences in the staining intensity were observed in the central retinas from mice of different genotypes (Fig. 4A and C).

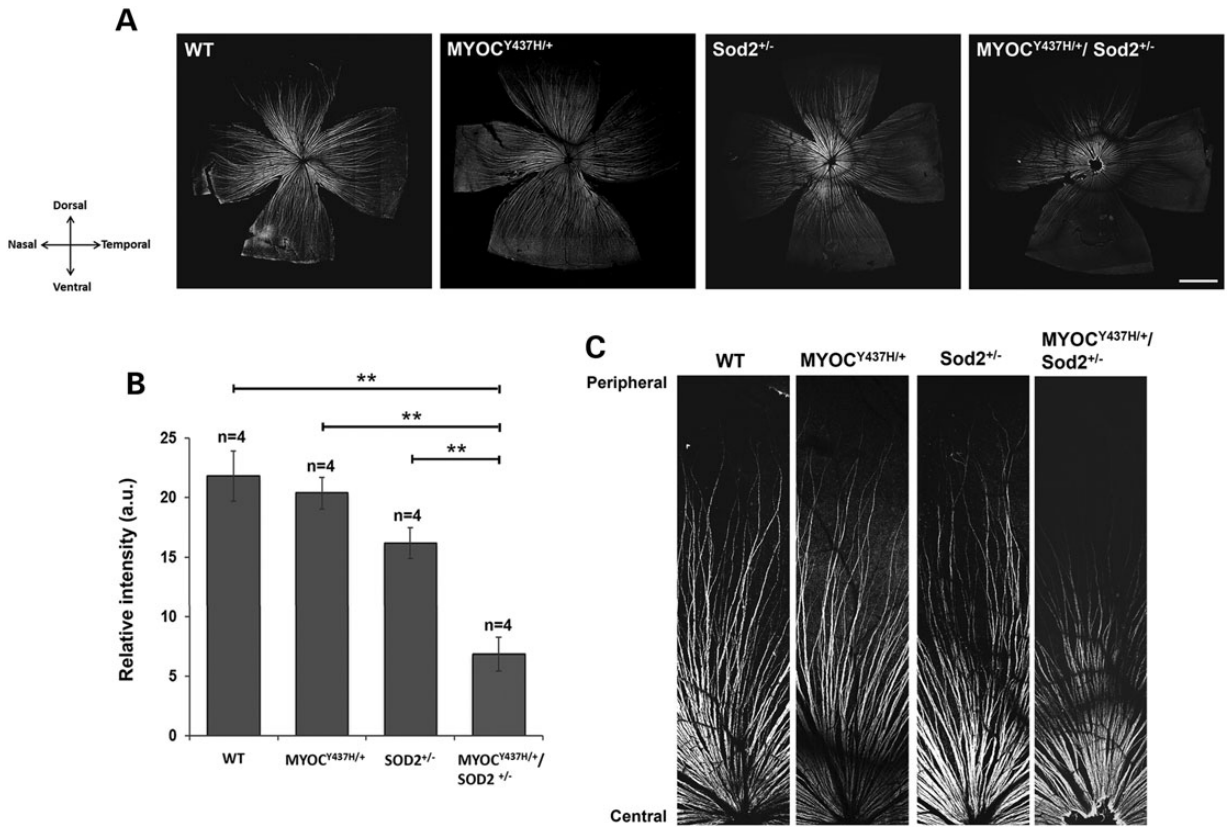

Figure 4. Neuronal fiber depletion in the retina of Tg-MYOC$^{Y437H/+}$/Sod2$^{+/-}$ mice. (**A**) Immunofluorescence of 10-month-old whole-mounted retinas stained with antibodies against NFH, which label RGC axons. Crossed arrows indicate the directions of the corresponding poles of the retinas. Four sets of littermate retinas were stained. Representative images are shown. Scale bar, 1 mm. (**B**) Relative fluorescence intensities of the NFH-staining of the entire whole-mounted retinas as in (A). All values are presented as mean ± SE. **$P < 0.01$. *n* shows the number of analyzed mice. (**C**) Higher magnification images of the dorsal retinas in (A) are shown from the central region (bottom) to the peripheral region (top).

To determine whether the Tg-MYOC$^{Y437H/+}$/Sod2$^{+/-}$ genotype is associated with elevated RGC death, we stained RGCs of 10- to 12-month-old mice of different genotypes with antibodies against NeuN and neuron-specific class III beta-tubulin (βIII TUB). Staining with two different markers similarly showed a decrease in the number of positive cells in the peripheral retinas of Tg-MYOC^{Y437H}/SOD2$^{+/-}$ mice (Fig. 5A). However, no significant differences were detected in the number of NeuN positive cells in the central retinas among mice with different genotypes (not shown). We used βIII TUB marker for further staining and quantitative analysis because this staining demonstrated the higher quality of images compared to NeuN staining. About 37% loss of βIII TUB-positive cells was detected in the peripheral retinas of Tg-MYOC$^{Y437H/+}$/Sod2$^{+/-}$ mice when compared with wild-type and single-mutant mice (Fig. 5B). These data revealed that Tg-MYOC$^{Y437H/+}$/Sod2$^{+/-}$ mice demonstrate elevated RGC death and axonal degeneration in the neuronal fiber layer when compared with wild-type littermates or mice carrying only a single mutation.

Cupping of the optic nerve head in Tg-MYOC$^{Y437H/+}$/Sod2$^{+/-}$ mice

Clinically, glaucomatous optic nerve damage is recognized by the enlargement and deepening of the optic cup. As glaucoma progresses, nerve fibers gradually die and the thickness of the neural fiber layer is diminished, causing the optic cup to enlarge. With fewer RGCs and depleted nerve fibers in the retinas of Tg-MYOC$^{Y437H/+}$/Sod2$^{+/-}$ mice, it seemed likely that the structure and appearance of the ONH as well as thickness of the neural fiber layer in the ONH area might show similar pathological changes. To assess changes in the ONH, whole retinas of 10-month-old mice were stained with antibodies against NFH and three-dimensional structures for the images of the ONH

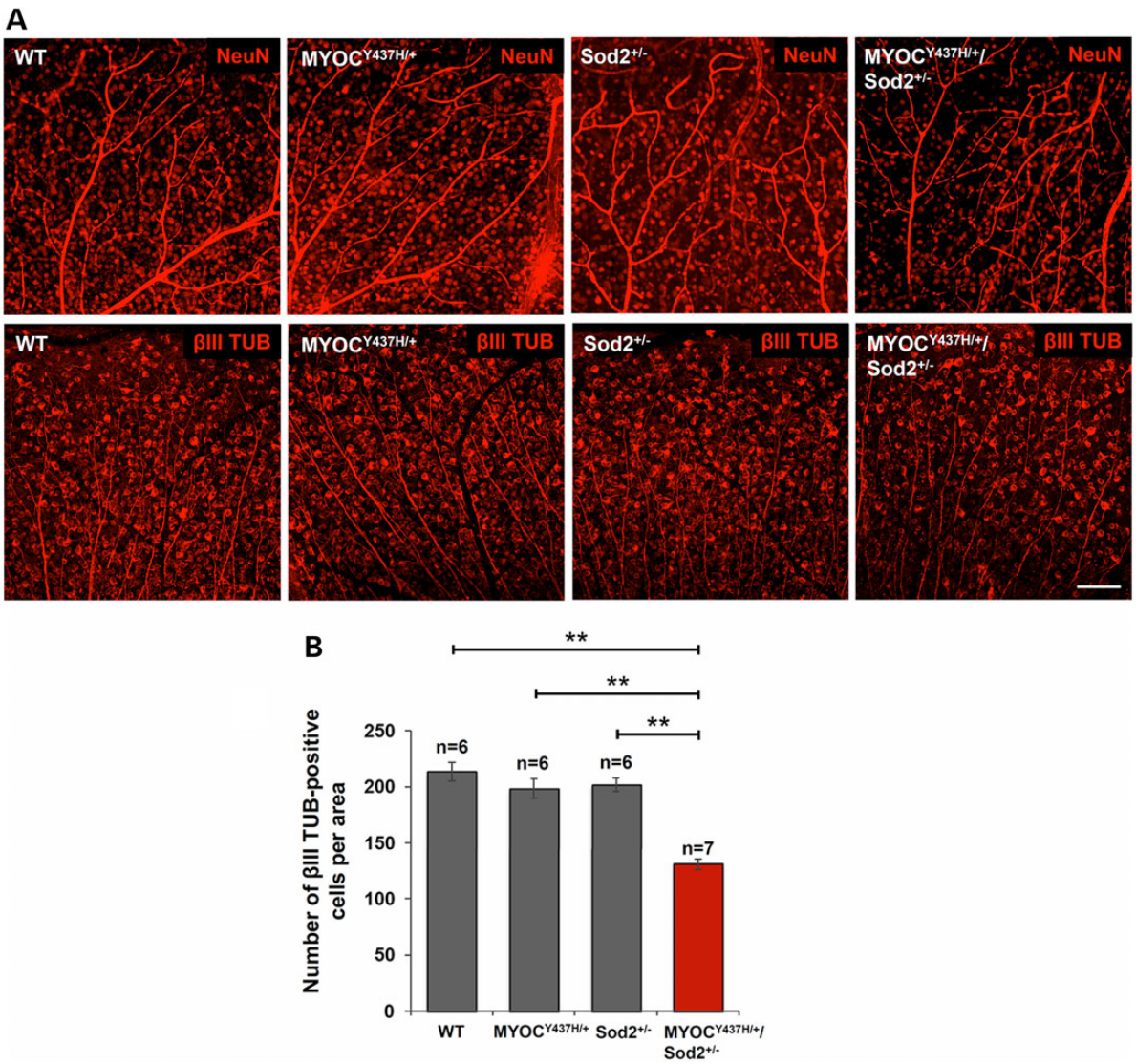

Figure 5. Loss of RGCs in the peripheral retinas of Tg-MYOC^{Y437H}/Sod2$^{+/-}$ mice. (**A**) RGCs were labeled by anti-NeuN (upper row) and anti-βIII TUB (lower row) antibodies in the whole-mounted retinas of 10-month-old littermates. Representative images from the peripheral retinas are shown. Scale bar, 100 μm. (**B**) βIII TUB-positive cells in the peripheral retinas of 10- to 12-month-old mice were counted and plotted as the numbers per area. All the values are presented as mean ± SE and analyzed by one-way ANOVA followed by Tukey's multiple comparisons test. $^{**}P < 0.01$; *n* shows the number of analyzed mice.

were constructed using confocal microscopy and the Volocity 3D analysis software. The boundary of NFH staining at the center of the whole retina reflected the size of the optic cup. The optic cup in the ONH was enlarged in Tg-MYOC$^{Y437H/+}$/Sod2$^{+/-}$ mice (Fig. 6A, upper panel). Furthermore, transverse sections showed thinning of the nerve fiber layer (Fig. 6A, lower panel and B) and a deeper excavation of the ONH in Tg-MYOC$^{Y437H/+}$/Sod2$^{+/-}$ mice (Fig. 6A, lower panel). Together, these findings indicate that cupping of the ONH occurs in Tg-MYOC$^{Y437H/+}$/Sod2$^{+/-}$ mice.

Axonal degeneration in the optic nerve of MYOC$^{Y437H/+}$/Sod2$^{+/-}$ mice

Degeneration of the optic nerve is one of the notable pathological changes in glaucoma patients. To identify degenerative changes in the optic nerves of mice with different genotypes, the ultrastructure of optic nerve transverse sections, cut at approximately 1 mm behind the globe, was analyzed in 10-month-old mice. Multiple pathological changes were detected throughout the optic nerve cross-sections of Tg-MYOC$^{Y437H/+}$/Sod2$^{+/-}$ mice. These changes included numerous demyelinated axons as well as additional features of axonal degeneration such as amorphous axoplasm, axolemma detachment, myelin debris and double myelination. In contrast, no significant pathological changes were seen in mice with the other genotypes (Fig. 7). Axonal degeneration of the optic nerve in Tg-MYOC$^{Y437H/+}$/Sod2$^{+/-}$ mice occurred earlier than in mice carrying only the Tg-MYOC$^{Y437H/+}$ mutation (20) and the edge area of the optic nerve is more affected than other areas of the optic nerve.

Elevated expression of ELAM-1, a molecular marker of human glaucoma, in the TM of Tg-MYOC$^{Y437H/+}$/SOD2$^{+/-}$ mice

ELAM-1, consistently detected in glaucomatous TM, is regarded as the first molecular marker of human glaucoma (43,44).

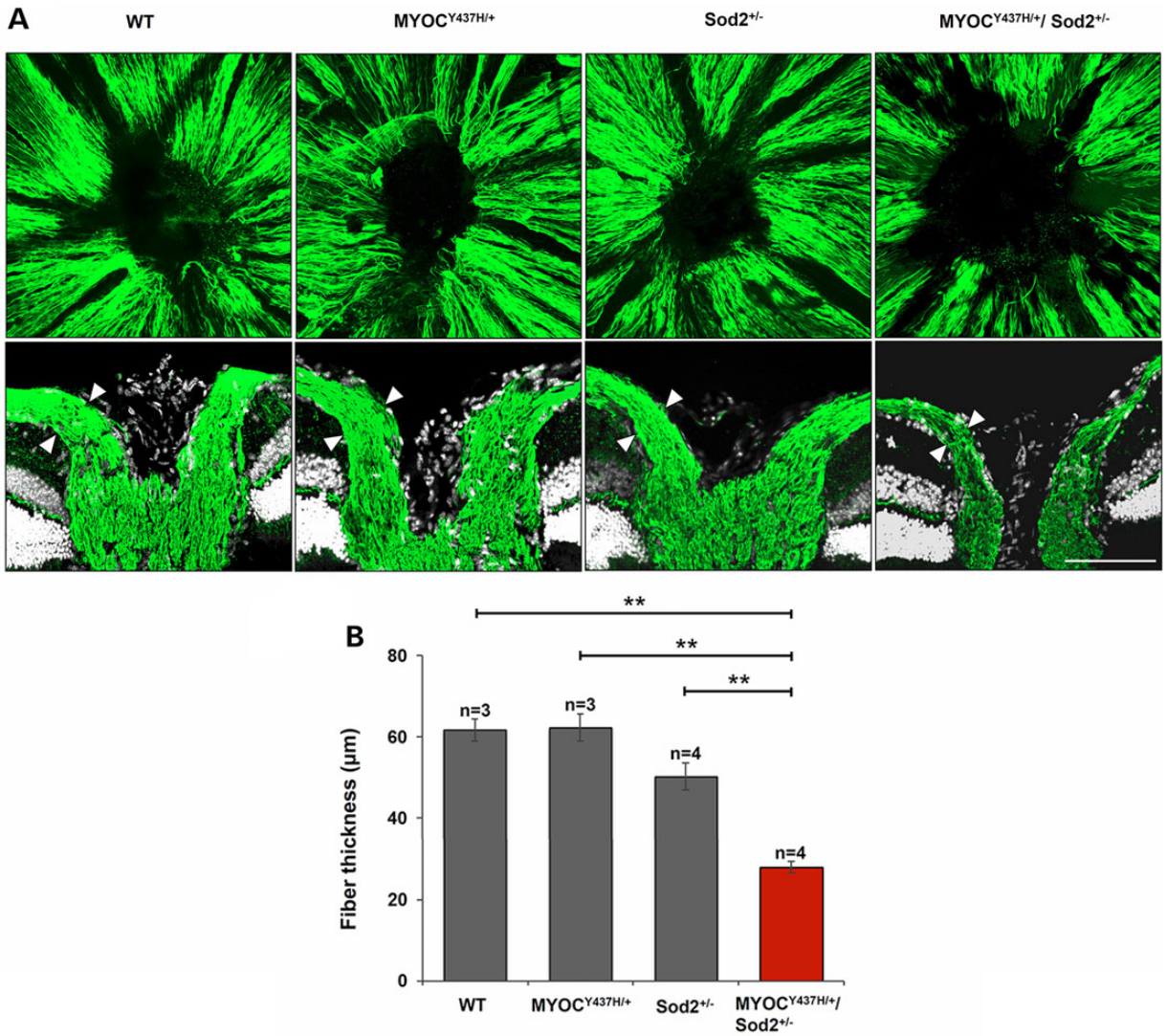

Figure 6. Nerve fiber layer atrophy and structural change in the ONH of Tg-MYOC$^{Y437H/+}$/Sod2$^{+/-}$ mice. Nerve fibers were labeled by anti-NFH antibodies in the whole-mounted retinas of 10-month-old littermates. 3D image stacks for nerve fiber layer in the ONH and surrounding areas of the retina are shown in the upper row. The corresponding transverse sections stained with antibodies against NFH and TO-PRO-3 are shown in the lower row. Similar results were obtained in three independent experiments. Representative stainings are shown. Scale bar, 100 μm. (**B**) Quantification of the nerve fiber layer thickness. The measurements were made at the points marked by the arrowheads in the lower set of images as in (**A**). All the values are presented as mean ± SE. $^{**}P < 0.01$. *n* shows the number of analyzed mice.

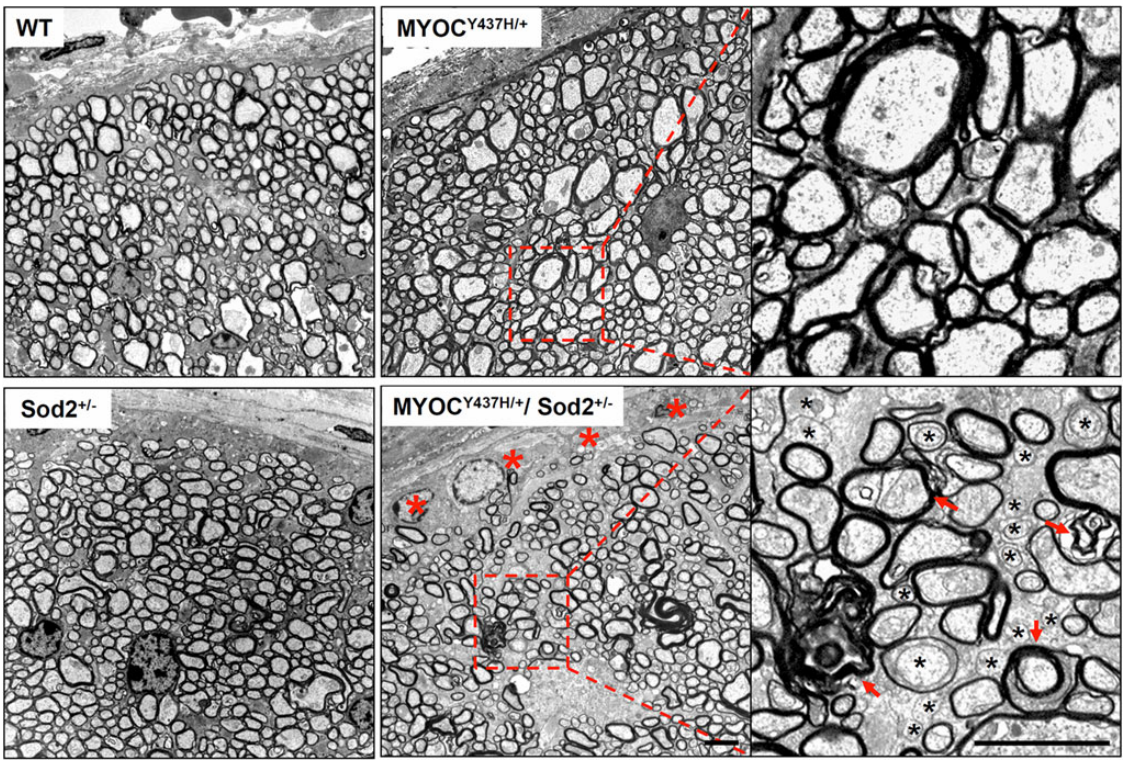

Figure 7. Degeneration in the optic nerves of Tg-MYOC$^{Y437H/+}$/Sod2$^{+/-}$ mice. Representative electron micrographs of the optic nerve cross-sections from 10-month-old littermates are shown. Red asterisks indicate the loss of axonal profiles in the edges of the optic nerve that were instead filled up with low-density material. Right panels show the higher magnification images for the areas marked by the red dotted line in the images from Tg-MYOC$^{Y437H/+}$ and Tg-MYOC$^{Y437H/+}$/Sod2$^{+/-}$ mice. Degenerating axons in the higher magnification image of Tg-MYOC$^{Y437H/+}$/Sod2$^{+/-}$ optic nerve were identified by the lack of myelin sheath (black asterisks) and the presence of amorphous axoplasm, axolemma detachment, myelin debris or double myelination (red arrows). Scale bars, 2 μm.

Up-regulation of *ELAM-1* mRNA in the TM of glaucomatous donors has been also demonstrated by microarray analysis (45), while a proteomic study demonstrated the presence of higher levels of ELAM-1 in the aqueous humor of POAG patients (46). Increased expression of ELAM-1 also has been reported in the aqueous outflow pathway of an induced glaucoma model (47). To test whether ELAM-1 is elevated in the TM of Tg-MYOC$^{Y437H/+}$/Sod2$^{+/-}$ mice, transverse sections of 8-month-old mouse eye were stained with antibodies against ELAM-1. ELAM-1 staining was significantly increased in the TM of Tg-MYOC$^{Y437H+/-}$/Sod2$^{+/-}$ mice and moderately increased in the TM of Tg-MYOC$^{Y437H+/-}$ mice as compared with staining of WT and Sod2$^{+/-}$ mice (Fig. 8A and B). Thus, the mice expressing the Y437H mutant myocilin indeed have up-regulated expression of a well-accepted marker for glaucoma, and the up-regulation is enhanced in Tg-MYOC$^{Y437H/+}$/Sod2$^{+/-}$mice.

Discussion

Adult-onset POAG is a complicated disease that appears to be influenced by multiple genetic and environmental factors (5,25). To date, at least 20 genetic loci have been identified as being associated with POAG. *MYOC* is the first identified and most studied glaucoma gene. The *MYOC* absence apparently does not lead to glaucoma (48,49). Disease-causing mutations in myocilin likely act by a gain of function mechanism (49). Available data suggest that myocilin-induced glaucoma can be a form of ER storage disease (23,50,51) and that disease pathogenesis in POAG patients depends upon the expression of abnormal mutated myocilin.

To study molecular mechanisms of myocilin-induced glaucoma, several mouse lines expressing Y437H human mutant myocilin or its corresponding mouse mutant, Y423H mouse mutant myocilin, in eye angle tissues have been produced. Two transgenic mouse lines expressing Y437H human mutant myocilin or its corresponding mouse mutant, Y423H mouse mutant myocilin have been generated using bacterial artificial chromosome DNA encoding the full-length human *MYOC* or mouse *Myoc* genes (20,21). These two mutant myocilin lines exhibited similar levels of pathological change, including approximately 2 mmHg higher IOP, a 20% loss of RGCs in the peripheral retina, and mild axonal degeneration in the optic nerve (20,21). In contrast to these results, replacement of the endogenous mouse *Myoc* allele with a mutant Y423H allele did not lead to an elevation of IOP and degenerative changes in the retina or optic nerve (22). This might be explained by different genetic backgrounds of mice (52) and/or different levels of mutant myocilin produced. Indeed, expression of high levels of mutated human Y437H myocilin in the eye drainage structures and sclera under the control of the cytomegalovirus promoter in transgenic mice led to elevation of IOP by about 3 mmHg at 3 months of age (23). This was accompanied by the loss of RGCs (about 18% by 3–5 months of age and 30% by 12–14 months of age) and optic nerve axons. Pathological changes observed in the eyes of mice expressing mutated myocilin are similar to those observed in glaucoma patients. However, pathological changes induced by the physiological levels of mutated myocilin are much less dramatic than the ones seen in human subjects with the same *MYOC* mutation. One possible explanation of the observed differences is that the conventional trabecular outflow pathway accounts for about 80% of aqueous humor removal in humans, while about 20% of aqueous humor leaves the eye through the

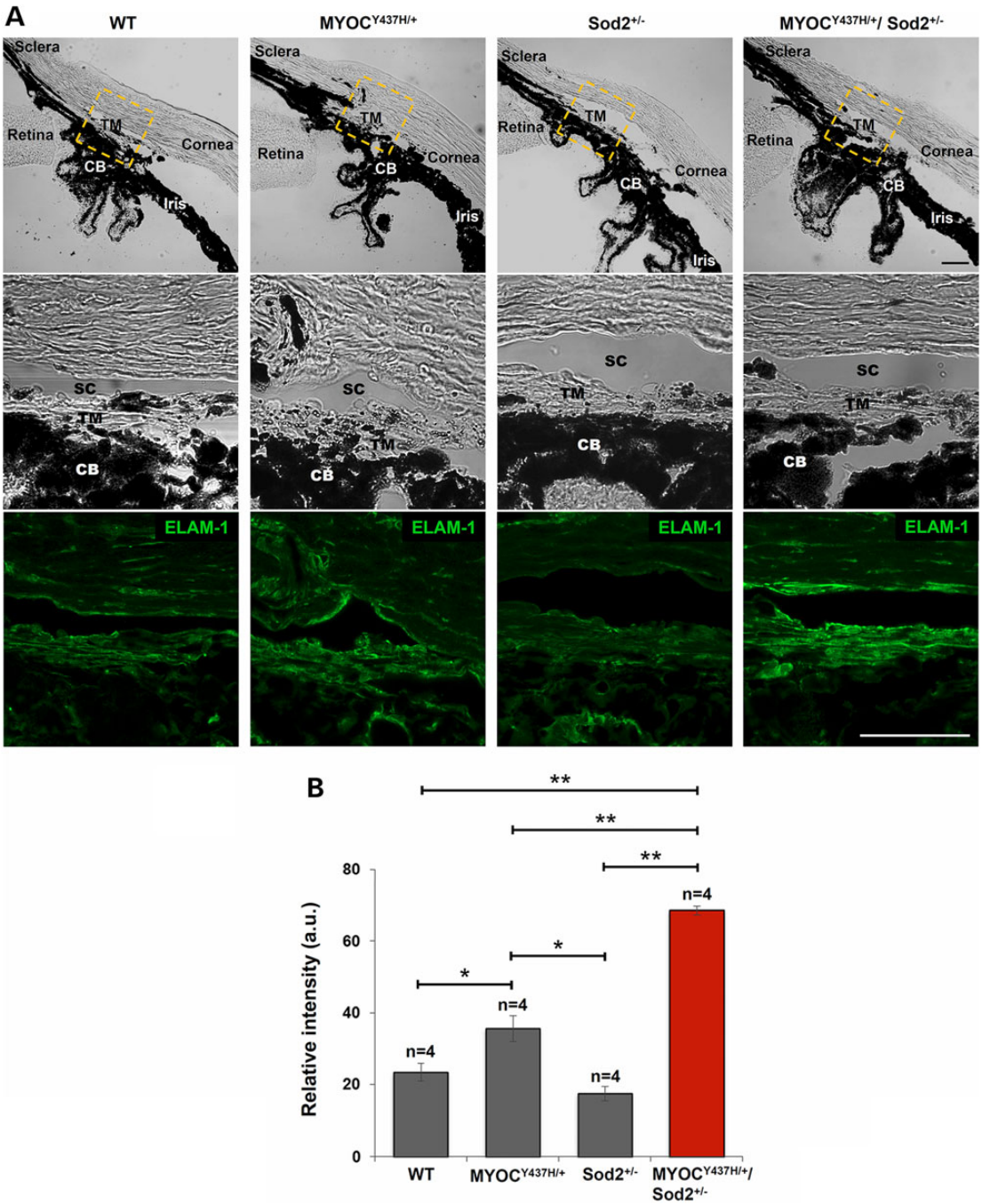

Figure 8. Increased expression of a human glaucoma marker, ELAM-1 in TM of Tg-MYOC$^{Y437H/+}$/Sod2$^{+/-}$ mice. Frozen eye sections of 8-month-old littermates were stained with antibodies against ELAM-1. The top panels show the bright-field images of the mouse iridocorneal angle. The middle (bright field) and bottom (ELAM-1 immunofluorescence) panels show the higher magnification for the area surrounded by yellow squares in the top panels. Similar results were obtained in three independent experiments. Representative stainings are shown. Scale bars, 50 μm; TM, trabecular meshwork; CB, ciliary body; SC, Schlemm's canal. (**B**) Quantification of ELAM-1 fluorescence intensities in the TM areas as in (**A**). All the values are presented as mean ± SE. *$P < 0.05$; **$P < 0.01$. *n* shows the number of analyzed mice.

unconventional uveoscleral pathway. In mice, oppositely, about 80% of aqueous humor leaves the eye through the uveoscleral pathway and only about 20% through the trabecular outflow pathway (53,54).

Although mutations in *MYOC* are considered to be a significant genetic factor, severity of the disease in individuals bearing a deleterious *MYOC* mutation may be dependent upon other risk factors during their life time. Patients with the Y437H mutation in MYOC demonstrate a range of recorded IOP (14–77 mm Hg) with mean 44 mm Hg as well as age at diagnosis of disease (8–41 years) with mean 20 years that is much earlier than typical age of non-MYOC-associated POAG (55). Mice may not be exposed to the same risk factors as humans due to a different life style. Moreover, since mice have a much shorter life span than humans, they might not be exposed to the risk factors long enough to lead to the severe pathological changes that humans acquire.

Therefore, to elevate pathological changes in a mouse model of glaucoma, mice carrying glaucoma-causing mutation in the *MYOC* gene could be exposed to additional risk factors or to an increased level of a particular risk factor.

Considerable evidence suggests that oxidative stress has an important role in the pathogenesis of glaucoma (56,57). Protein misfolding and oxidative stress are closely related events (29). Accumulation of unfolded proteins in the ER lumens causes oxidative stress, while ROS by itself can cause protein misfolding and the ER (58). Expression of mutated myocilin sensitizes cells to oxidative stress and leads to cell death, even at low oxidant concentrations, suggesting that oxidative stress, a risk factor and a component of the aging process, together with mutated myocilin may produce more severe glaucoma than any of these factors alone (16). TM, a tissue that contains high levels of myocilin, is the tissue in the anterior chamber that is most sensitive to oxidative damage (59). Therefore, the TM may be most sensitive to the synergistic effects of mutated myocilin and oxidative stress. Indeed, Tg-MYOC$^{Y437H/+}$/Sod2$^{+/-}$ double-mutant mice showed severe ER stress in eye drainage structures that ultimately resulted in cell death in the TM. This suggests that the deleterious effect of mutated myocilin may lead to a reduction in the number of TM cells in an environment of higher-level oxidative stress in humans. Clinical research has shown that TM cell loss can correlate with POAG progression. POAG patients have lower TM cellularity compared to normal age-matched controls (60), and this cellularity declines with age (61,62). Reduction in the number of TM cells may be associated with TM dysfunction and, subsequently, increased IOP in humans. Our 10- to 12-month-old Tg-MYOC$^{Y437H/+}$/Sod2$^{+/-}$ mice showed about 45% reduction in the amount of TM cells as compared with single mutants or with wild-type, while a single Tg-MYOC$^{Y437H/+}$ mutant showed only moderate non-statistically significant reduction of TM cells when compared with wild-type. We also demonstrated that actin fibers are reduced in the TM of Tg-MYOC$^{Y437H/+}$/Sod2$^{+/-}$ mice. TM cells have a distinct actomyosin cytoskeleton and exhibit considerable contractile properties. The contractility of the actomyosin system in TM cells or the inner wall endothelium of Schlemm's canal is an important determinant in the regulation of outflow resistance (63). IOP elevation most often appears to be caused by an increased resistance to the outflow of aqueous humor through the drainage structures. The reduced actin fibers observed when alpha-actin positive cells are themselves reduced may lead to a decline in contractility of the actomyosin system and malfunction of the TM, which in turn can cause elevated IOP. We identified much higher IOP in Tg-MYOC$^{Y437H/+}$/Sod2$^{+/}$ mice at 8 months of age than that in Tg-MYOC$^{Y437H/+}$ mice at 18 months of age (20). This again indicates that the combination of mutated *MYOC* and *Sod2* haplodeficience accelerates the onset of disease. Eight months in mice is an equivalent of 22–23 years of human life (64). This age is close to the average age at which glaucoma is diagnosed among human patients with the MYOC$^{Y437H/+}$ mutations. However, the absolute or relative increase in IOP of Tg-MYOC$^{Y437H/+}$/Sod2$^{+/-}$ mice is still smaller than those observed in patients with the same *MYOC* mutation. Although IOP was not dramatically elevated, we observed pronounced pathological glaucomatous changes in the retina and optic nerve of Tg-MYOC$^{Y437H/+}$/Sod2$^{+/-}$ mice.

Growing evidence suggests involvement of the ROS in RGC death and axonal degeneration in the retina (56). For example, a study of homozygous *Sod2* knockout mice revealed thinning of the total retina, including nerve fibers and the RGC layer (65). In the current study, we also identified moderate depletion of the nerve fibers in the retina of *Sod2* haplodeficient mice, though this depletion as well as changes in the retinal thickness or the RGC number in 10- to 12-month-old *Sod2* haplodeficient mice were not statistically significant. This insinuates that higher levels of ROS in the retina may also contribute to retinal deterioration. As such, RGCs and their axons, when slightly damaged by oxidative stress, may be more vulnerable to mechanical stresses produced by elevated IOP. The depletion in retinal nerve fibers and loss of RGCs in the retina of Tg-MYOC$^{Y437H/+}$/Sod2$^{+/-}$ mice were not evenly distributed throughout the whole retina, just as glaucomatous damage in human patients is not usually evenly distributed. Interestingly, healthy individuals also exhibit varying thickness of retinal nerve fibers, depending on the sector of retina. Sectorial degeneration of axons was similarly observed in the DBA/2J mouse glaucoma model and rat ocular hypertension model (66,67). Glaucomatous retinal damage was mainly detected in the peripheral retina of Tg-MYOC$^{Y437H/+}$/Sod2$^{+/-}$ mice. This observation is compatible with the pattern of disease progression observed in other mouse models of glaucoma (20,21,68) and human glaucoma patients, in which glaucoma most often affects peripheral visual function at its early stages, while deterioration of the central retina generally is only seen at the later stages of disease.

We believe that the mouse glaucoma model induced by the combination of glaucoma-associated mutated myocilin and a second risk factor (oxidative stress) may more closely mimic the complicated pathogenic mechanisms that arise in human glaucoma patients. It is well established that UV light, ionizing radiation, chemotherapeutics, and environmental toxins are exogenous sources of ROS. Smoking, another cause of high oxidative stress (69), has been identified as a risk factor in elder women with POAG (70). Antioxidant drug therapy approaches were suggested and tested for neuroprotection in glaucoma (71–73). Antioxidant drug approaches could be also beneficial for patients with glaucoma-causing myocilin mutations who should avoid the substances and behavior such as smoking causing free radical production and may try antioxidants to delay the progression of the disease.

Materials and Methods

Production of double-mutant mice

Heterozygous *Sod2* null mice (original strain name: B6.129S7-Sod2^{tm1Leb}/J) were purchased from the Jackson Laboratories (Bar Harbor, ME). Tg-MYOC$^{Y437H/+}$ have been previously described (20). Heterozygous *Sod2* null and Tg-MYOC$^{Y437H/+}$ mice were mated with C57/BL6 mice for at least five generations. All further matings between different mouse lines were conducted with F5 and later generations. To generate doubly heterozygous (Tg-MYOC$^{Y437H/+}$/Sod2$^{+/-}$) mice, Tg-MYOC$^{Y437H/+}$ mice were mated with Sod2$^{+/-}$mice. Mice were maintained in accordance with guidelines set forth by the National Eye Institute Committee on the Use and Care of Animals and the Association for Research in Vision and Ophthalmology's Statement for the Use of Animals in Ophthalmic and Visual Research.

IOP measurement

Mice were anesthetized with a mixture of ketamine (100 mg/kg) and xylazine (10 mg/kg). IOP was measured in anesthetized animals using a fiber-optic signal (FTI-10) conditioner equipped with a fiber-optic pressure transducer (FISO Technologies, Montreal, Quebec, Canada) as described previously (20,21). The measurements were made from 9 AM to noon. IOP from each eye was

recorded during a 2-min session, with four measurements taken at 30-sec intervals within each session. The average of these four measurements was used to calculate IOP for each eye. Dacriose sterile eye irrigation solution (Novartis, Basel, Switzerland) was topically applied after each IOP measurement.

Immunoblotting

The mouse iridocorneal angle tissues (the ciliary body, TM, and base of the iris and cornea) were dissected, homogenized in the lysis buffer (50 mM Tris, pH 7.5, 5 mM EDTA, 20 mM dithiothreitol, 0.2% SDS, 1% Triton X-100, and 1% Tween 20), and centrifuged to remove insoluble material. Proteins of the soluble fraction (20 μg) were separated by NuPAGE 4–12% gradient Bis-Tris gel (Life Technologies, Frederick, MD, USA) and transferred to a nitrocellulose membrane (Life Technologies). Membranes were pre-incubated in a blocking buffer (5% nonfat milk, 25 mM Tris, pH 7.4, 150 mM NaCl, 0.05% Tween 20) and then incubated with antibodies against myocilin (1:4000) (49), GRP78 (1:500; Cell Signaling Technology, Beverly, MA, USA), Bim (1:500; Cell Signaling Technology), cleaved PARP (1:500; Cell Signaling Technology) or heat-shock cognate 70 (HSC70; 1:2000; Santa Cruz Biotechnology, Santa Cruz, CA, USA) in blocking buffer overnight at 4°C. Secondary antibodies (an anti-rabbit or anti-mouse horseradish peroxidase antibodies; Amersham, Piscataway, NJ, USA) were diluted 1:5000 in a blocking buffer and incubated for 2 h at room temperature. The immunoreactive bands were developed by using SuperSignal West Dura or West Femto chemiluminescent substrate (Pierce, Rockford, IL, USA). For the quantification, images were analyzed using Image J software (NIH, Bethesda, MD, USA).

Immunofluorescent labeling and image analysis

Mouse eyes were fixed in 4% paraformaldehyde for 2 h before processing for cryosection embedding or whole-tissue preparation. Frozen sections (10 μm) of mouse eyes were blocked in a blocking buffer (2% normal goat serum and 0.2% Triton X-100 in PBS) for 1 h and incubated with antibodies against GRP78 (1:100; Cell Signaling Technology), α-SMA (1:200; Abcam, Cambridge, MA) or NFH (1:200; EMD Millipore, Temecula, CA) in a blocking buffer for 3 h, followed by incubation with Alexa 488-conjugated anti-rabbit secondary antibody (1:500; Life Technologies) for 1 h. Sections were mounted in the ProLong Gold antifade reagent (Life Technologies) or further incubated for 3 h with anti-myocilin antibody which was pre-labeled with DyLight 594 fluorescent dye (74). Whole eye balls, whole retinas or dissected anterior segments were blocked in a blocking buffer (1% normal goat serum, 1% BSA and 1% Triton X-100 in PBS) for 1 h and incubated with antibodies against α-SMA (1:100; Abcam), NFH (1:200; EMD Millipore), or βIII TUB (1:100; Covance, Berkeley, CA, USA) for 48 h at 4°C, followed by incubation with Alexa 488 (or 555) goat anti-rabbit secondary antibody (1:500; Life Technologies) or Alexa 488 goat anti-rat secondary antibody (1:500; Life Technologies) for 24 h at 4°C. The mounted samples were examined, and fluorescent images were collected using a Zeiss LSM 700 confocal microscope (Zeiss, Jena, Germany).

The images of α-SMA-positive areas in anterior segments were acquired using the tile scan function (1 × 3 tiles). For the quantification of TM cells, TO-PRO-3 (Life Technologies)-stained nuclei in α-SMA-positive TM areas were counted from three randomly selected areas of 50 × 50 μm in the acquired images. The average of three measurements was used to compare different animals. To quantify RGCs, images from each of the four retinal segments were randomly selected to count the number of βIII TUB-positive cells per an area of 375 × 375 μm. The average of the four measurements was used to compare different animals. Fluorescence intensities of the entire NFH-stained whole-mount retinas were measured using ZEN Software 2012 (Carl Zeiss). To quantify ELAM-1 fluorescence intensity in TM, TM area was selected and fluorescence quantification was performed as described above. To compare the structures of ONH, confocal z-stacks were collected at 0.271 μm intervals from ONH in the NFH-stained whole retinas. 3D reconstructions from 90 optical sections were performed using Volocity software (PerkinElmer, Waltham, MA, USA). The nerve fiber layer thickness near the ONH was measured using ZEN Software 2012 (Carl Zeiss).

Electron microscopy

Retrobulbar optic nerve segments were double-fixed in 2.5% glutaraldehyde and 0.5% osmium tetroxide in PBS, dehydrated, and embedded in Spurr's epoxy resin. Ultrathin sections (90 nm) were prepared, double-stained with uranyl acetate and lead citrate, and viewed in a JEOL JEM-1010 transmission electron microscope equipped with digital imaging camera.

Statistical analysis

Quantitative data were presented as mean ± S.E. Statistical analysis for two groups was performed using a two-tailed Student's t-test. Statistical analysis for multiple groups was performed with one-way factorial analysis of variance (ANOVA) and subsequent Tukey's multiple comparison test. In all statistical analyses, significance was defined as $P < 0.05$.

Acknowledgements

We thank Dr Cynthia Jaworski for critical reading of the manuscript.

Conflict of Interest statement. None declared.

Funding

This work was supported by the Intramural Research Programs of the National Eye Institute, National Institutes of Health.

References

1. Quigley, H.A. and Broman, A.T. (2006) The number of people with glaucoma worldwide in 2010 and 2020. *Br. J. Ophthalmol.*, **90**, 262–267.
2. Rivera, J.L., Bell, N.P. and Feldman, R.M. (2008) Risk factors for primary open angle glaucoma progression: what we know and what we need to know. *Curr. Opin. Ophthalmol.*, **19**, 102–106.
3. Tham, Y.C., Li, X., Wong, T.Y., Quigley, H.A., Aung, T. and Cheng, C.Y. (2014) Global prevalence of glaucoma and projections of glaucoma burden through 2040: a systematic review and meta-analysis. *Ophthalmology.*, **121**, 2081–2090.
4. Francois, J. (1981) Genetic predisposition to glaucoma. *Dev. Ophthalmol.*, **3**, 1–45.
5. Fan, B.J. and Wiggs, J.L. (2010) Glaucoma: genes, phenotypes, and new directions for therapy. *J. Clin. Invest.*, **120**, 3064–3072.
6. Shimizu, S., Lichter, P.R., Johnson, A.T., Zhou, Z., Higashi, M., Gottfredsdottir, M., Othman, M., Moroi, S.E., Rozsa, F.W., Schertzer, R.M. *et al.* (2000) Age-dependent prevalence of mutations at the GLC1A locus in primary open-angle glaucoma. *Am. J. Ophthalmol.*, **130**, 165–177.

7. Wiggs, J.L., Allingham, R.R., Vollrath, D., Jones, K.H., De La Paz, M., Kern, J., Patterson, K., Babb, V.L., Del Bono, E.A., Broomer, B.W. *et al.* (1998) Prevalence of mutations in TIGR/Myocilin in patients with adult and juvenile primary open-angle glaucoma. *Am. J. Hum. Genet.*, **63**, 1549–1552.
8. Fingert, J.H., Heon, E., Liebmann, J.M., Yamamoto, T., Craig, J. E., Rait, J., Kawase, K., Hoh, S.T., Buys, Y.M., Dickinson, J. *et al.* (1999) Analysis of myocilin mutations in 1703 glaucoma patients from five different populations. *Hum. Mol. Genet.*, **8**, 899–905.
9. Hewitt, A.W., Mackey, D.A. and Craig, J.E. (2008) Myocilin allele-specific glaucoma phenotype database. *Hum. Mutat.*, **29**, 207–211.
10. Jacobson, N., Andrews, M., Shepard, A.R., Nishimura, D., Searby, C., Fingert, J.H., Hageman, G., Mullins, R., Davidson, B.L., Kwon, Y.H. *et al.* (2001) Non-secretion of mutant proteins of the glaucoma gene myocilin in cultured trabecular meshwork cells and in aqueous humor. *Hum. Mol. Genet.*, **10**, 117–125.
11. Zhou, Z. and Vollrath, D. (1999) A cellular assay distinguishes normal and mutant TIGR/myocilin protein. *Hum. Mol. Genet.*, **8**, 2221–2228.
12. Orwig, S.D., Perry, C.W., Kim, L.Y., Turnage, K.C., Zhang, R., Vollrath, D., Schmidt-Krey, I. and Lieberman, R.L. (2012) Amyloid fibril formation by the glaucoma-associated olfactomedin domain of myocilin. *J. Mol .Biol.*, **421**, 242–255.
13. Joe, M.K., Sohn, S., Hur, W., Moon, Y., Choi, Y.R. and Kee, C. (2003) Accumulation of mutant myocilins in ER leads to ER stress and potential cytotoxicity in human trabecular meshwork cells. *Biochem. Biophys. Res. Commun.*, **312**, 592–600.
14. Liu, Y. and Vollrath, D. (2004) Reversal of mutant myocilin non-secretion and cell killing: implications for glaucoma. *Hum. Mol. Genet.*, **13**, 1193–1204.
15. Yam, G.H., Gaplovska-Kysela, K., Zuber, C. and Roth, J. (2007) Aggregated myocilin induces russell bodies and causes apoptosis: implications for the pathogenesis of myocilin-caused primary open-angle glaucoma. *Am. J. Pathol.*, **170**, 100–109.
16. Joe, M.K. and Tomarev, S.I. (2010) Expression of myocilin mutants sensitizes cells to oxidative stress-induced apoptosis: implication for glaucoma pathogenesis. *Am. J. Pathol.*, **176**, 2880–2890.
17. Kwon, Y.H., Fingert, J.H., Kuehn, M.H. and Alward, W.L. (2009) Primary open-angle glaucoma. *N. Engl. J. Med.*, **360**, 1113–1124.
18. Tomarev, S.I., Wistow, G., Raymond, V., Dubois, S. and Malyukova, I. (2003) Gene expression profile of the human trabecular meshwork: NEIBank sequence tag analysis. *Invest. Ophthalmol. Vis. Sci.*, **44**, 2588–2596.
19. Tamm, E.R., Russell, P., Epstein, D.L., Johnson, D.H. and Piatigorsky, J. (1999) Modulation of myocilin/TIGR expression in human trabecular meshwork. *Invest. Ophthalmol. Vis. Sci.*, **40**, 2577–2582.
20. Zhou, Y., Grinchuk, O. and Tomarev, S.I. (2008) Transgenic mice expressing the Tyr437His mutant of human myocilin protein develop glaucoma. *Invest. Ophthalmol. Vis. Sci.*, **49**, 1932–1939.
21. Senatorov, V., Malyukova, I., Fariss, R., Wawrousek, E.F., Swaminathan, S., Sharan, S.K. and Tomarev, S. (2006) Expression of mutated mouse myocilin induces open-angle glaucoma in transgenic mice. *J. Neurosci.*, **26**, 11903–11914.
22. Gould, D.B., Reedy, M., Wilson, L.A., Smith, R.S., Johnson, R.L. and John, S.W. (2006) Mutant myocilin nonsecretion in vivo is not sufficient to cause glaucoma. *Mol. Cell. Biol.*, **26**, 8427–8436.
23. Zode, G.S., Kuehn, M.H., Nishimura, D.Y., Searby, C.C., Mohan, K., Grozdanic, S.D., Bugge, K., Anderson, M.G., Clark, A.F., Stone, E.M. *et al.* (2011) Reduction of ER stress via a chemical chaperone prevents disease phenotypes in a mouse model of primary open angle glaucoma. *J. Clin. Invest.*, **121**, 3542–3553.
24. Charliat, G., Jolly, D. and Blanchard, F. (1994) Genetic risk factor in primary open-angle glaucoma: a case-control study. *Ophthalmic. Epidemiol.*, **1**, 131–138.
25. Janssen, S.F., Gorgels, T.G., Ramdas, W.D., Klaver, C.C., van Duijn, C.M., Jansonius, N.M. and Bergen, A.A. (2013) The vast complexity of primary open angle glaucoma: disease genes, risks, molecular mechanisms and pathobiology. *Prog. Retin. Eye Res.*, **37**, 31–67.
26. Fan, B.J., Leung, Y.F., Wang, N., Lam, S.C., Liu, Y., Tam, O.S. and Pang, C.P. (2004) Genetic and environmental risk factors for primary open-angle glaucoma. *Chin. Med. J.*, **117**, 706–710.
27. Wiggs, J.L. (2012) The cell and molecular biology of complex forms of glaucoma: updates on genetic, environmental, and epigenetic risk factors. *Invest. Ophthalmol. Vis. Sci.*, **53**, 2467–2469.
28. Aseervatham, G.S., Sivasudha, T., Jeyadevi, R. and Arul Ananth, D. (2013) Environmental factors and unhealthy lifestyle influence oxidative stress in humans—an overview. *Environ. Sci. Pollut. Res. Int.*, **20**, 4356–4369.
29. Malhotra, J.D. and Kaufman, R.J. (2007) Endoplasmic reticulum stress and oxidative stress: a vicious cycle or a double-edged sword? *Antioxid. Redox Signal.*, **9**, 2277–2293.
30. He, Y., Leung, K.W., Zhuo, Y.H. and Ge, J. (2009) Pro370Leu mutant myocilin impairs mitochondrial functions in human trabecular meshwork cells. *Mol. Vis.*, **15**, 815–825.
31. Fridovich, I. (1995) Superoxide radical and superoxide dismutases. *Annu. Rev. Biochem.*, **64**, 97–112.
32. Gonzalez, P., Epstein, D.L. and Borras, T. (2000) Characterization of gene expression in human trabecular meshwork using single-pass sequencing of 1060 clones. *Invest. Ophthalmol. Vis. Sci.*, **41**, 3678–3693.
33. Ahmed, F., Torrado, M., Zinovieva, R.D., Senatorov, V.V., Wistow, G. and Tomarev, S.I. (2004) Gene expression profile of the rat eye iridocorneal angle: NEIBank expressed sequence tag analysis. *Invest. Ophthalmol. Vis. Sci.*, **45**, 3081–3090.
34. Li, Y., Huang, T.T., Carlson, E.J., Melov, S., Ursell, P.C., Olson, J. L., Noble, L.J., Yoshimura, M.P., Berger, C., Chan, P.H. *et al.* (1995) Dilated cardiomyopathy and neonatal lethality in mutant mice lacking manganese superoxide dismutase. *Nat. Genet.*, **11**, 376–381.
35. Van Remmen, H., Ikeno, Y., Hamilton, M., Pahlavani, M., Wolf, N., Thorpe, S.R., Alderson, N.L., Baynes, J.W., Epstein, C.J., Huang, T.T. *et al.* (2003) Life-long reduction in MnSOD activity results in increased DNA damage and higher incidence of cancer but does not accelerate aging. *Physiol. Genomics*, **16**, 29–37.
36. Van Remmen, H., Salvador, C., Yang, H., Huang, T.T., Epstein, C.J. and Richardson, A. (1999) Characterization of the antioxidant status of the heterozygous manganese superoxide dismutase knockout mouse. *Arch. Biochem. Biophys.*, **363**, 91–97.
37. Wan, X.S., Devalaraja, M.N. and St Clair, D.K. (1994) Molecular structure and organization of the human manganese superoxide dismutase gene. *DNA Cell Biol.*, **13**, 1127–1136.
38. Puthalakath, H., O'Reilly, L.A., Gunn, P., Lee, L., Kelly, P.N., Huntington, N.D., Hughes, P.D., Michalak, E.M., McKimm-Breschkin, J., Motoyama, N. *et al.* (2007) ER stress triggers apoptosis by activating BH3-only protein Bim. *Cell*, **129**, 1337–1349.
39. Kaufmann, S.H., Desnoyers, S., Ottaviano, Y., Davidson, N.E. and Poirier, G.G. (1993) Specific proteolytic cleavage of poly

(ADP-ribose) polymerase: an early marker of chemotherapy-induced apoptosis. *Cancer Res.*, **53**, 3976–3985.
40. de Kater, A.W., Shahsafaei, A. and Epstein, D.L. (1992) Localization of smooth muscle and nonmuscle actin isoforms in the human aqueous outflow pathway. *Invest. Ophthalmol. Vis. Sci.*, **33**, 424–429.
41. Gabelt, B.T. and Kaufman, P.L. (2005) Changes in aqueous humor dynamics with age and glaucoma. *Prog. Retin. Eye Res.*, **24**, 612–637.
42. Savinova, O.V., Sugiyama, F., Martin, J.E., Tomarev, S.I., Paigen, B.J., Smith, R.S. and John, S.W. (2001) Intraocular pressure in genetically distinct mice: an update and strain survey. *BMC Genet.*, **2**, 12.
43. Wang, N., Chintala, S.K., Fini, M.E. and Schuman, J.S. (2001) Activation of a tissue-specific stress response in the aqueous outflow pathway of the eye defines the glaucoma disease phenotype. *Nat. Med.*, **7**, 304–309.
44. Tomarev, S.I. (2001) Eyeing a new route along an old pathway. *Nat. Med.*, **7**, 294–295.
45. Liton, P.B., Luna, C., Challa, P., Epstein, D.L. and Gonzalez, P. (2006) Genome-wide expression profile of human trabecular meshwork cultured cells, nonglaucomatous and primary open angle glaucoma tissue. *Mol. Vis.*, **12**, 774–790.
46. Sacca, S.C., Centofanti, M. and Izzotti, A. (2012) New proteins as vascular biomarkers in primary open angle glaucomatous aqueous humor. *Invest. Ophthalmol. Vis. Sci.*, **53**, 4242–4253.
47. Suarez, T. and Vecino, E. (2006) Expression of endothelial leukocyte adhesion molecule 1 in the aqueous outflow pathway of porcine eyes with induced glaucoma. *Mol. Vis.*, **12**, 1467–1472.
48. Lam, D.S., Leung, Y.F., Chua, J.K., Baum, L., Fan, D.S., Choy, K. W. and Pang, C.P. (2000) Truncations in the TIGR gene in individuals with and without primary open-angle glaucoma. *Invest. Ophthalmol. Vis. Sci.*, **41**, 1386–1391.
49. Kim, B.S., Savinova, O.V., Reedy, M.V., Martin, J., Lun, Y., Gan, L., Smith, R.S., Tomarev, S.I., John, S.W. and Johnson, R.L. (2001) Targeted disruption of the Myocilin Gene (Myoc) suggests that human glaucoma-causing mutations are gain of function. *Mol. Cell. Biol.*, **21**, 7707–7713.
50. Suntharalingam, A., Abisambra, J.F., O'Leary, J.C. 3rd, Koren, J. 3rd, Zhang, B., Joe, M.K., Blair, L.J., Hill, S.E., Jinwal, U.K., Cockman, M. *et al.* (2012) Glucose-regulated protein 94 triage of mutant myocilin through endoplasmic reticulum-associated degradation subverts a more efficient autophagic clearance mechanism. *J. Biol. Chem.*, **287**, 40661–40669.
51. Anholt, R.R. and Carbone, M.A. (2013) A molecular mechanism for glaucoma: endoplasmic reticulum stress and the unfolded protein response. *Trends Mol. Med.*, **19**, 586–593.
52. McDowell, C.M., Luan, T., Zhang, Z., Putliwala, T., Wordinger, R.J., Millar, J.C., John, S.W., Pang, I.H. and Clark, A.F. (2012) Mutant human myocilin induces strain specific differences in ocular hypertension and optic nerve damage in mice. *Exp. Eye. Res.*, **100**, 65–72.
53. Alm, A. and Nilsson, S.F. (2009) Uveoscleral outflow—a review. *Exp. Eye Res.*, **88**, 760–768.
54. Aihara, M., Lindsey, J.D. and Weinreb, R.N. (2003) Aqueous humor dynamics in mice. *Invest. Ophthalmol. Vis. Sci.*, **44**, 5168–5173.
55. Alward, W.L., Fingert, J.H., Coote, M.A., Johnson, A.T., Lerner, S.F., Junqua, D., Durcan, F.J., McCartney, P.J., Mackey, D.A., Sheffield, V.C. *et al.* (1998) Clinical features associated with mutations in the chromosome 1 open-angle glaucoma gene (GLC1A). *N. Engl. J. Med.*, **338**, 1022–1027.
56. Izzotti, A., Bagnis, A. and Sacca, S.C. (2006) The role of oxidative stress in glaucoma. *Mutat. Res.*, **612**, 105–114.
57. Tezel, G. (2006) Oxidative stress in glaucomatous neurodegeneration: mechanisms and consequences. *Prog. Retin. Eye Res.*, **25**, 490–513.
58. Malhotra, J.D., Miao, H., Zhang, K., Wolfson, A., Pennathur, S., Pipe, S.W. and Kaufman, R.J. (2008) Antioxidants reduce endoplasmic reticulum stress and improve protein secretion. *Proc. Natl. Acad. Sci. USA*, **105**, 18525–18530.
59. Izzotti, A., Sacca, S.C., Longobardi, M. and Cartiglia, C. (2009) Sensitivity of ocular anterior chamber tissues to oxidative damage and its relevance to the pathogenesis of glaucoma. *Invest. Ophthalmol. Vis. Sci.*, **50**, 5251–5258.
60. Alvarado, J., Murphy, C. and Juster, R. (1984) Trabecular meshwork cellularity in primary open-angle glaucoma and nonglaucomatous normals. *Ophthalmology*, **91**, 564–579.
61. Grierson, I. and Howes, R.C. (1987) Age-related depletion of the cell population in the human trabecular meshwork. *Eye (Lond)*, **1**, 204–210.
62. Alvarado, J., Murphy, C., Polansky, J. and Juster, R. (1981) Age-related changes in trabecular meshwork cellularity. *Invest. Ophthalmol. Vis. Sci.*, **21**, 714–727.
63. Tian, B., Gabelt, B.T., Geiger, B. and Kaufman, P.L. (2009) The role of the actomyosin system in regulating trabecular fluid outflow. *Exp. Eye. Res.*, **88**, 713–717.
64. Demetrius, L. (2006) Aging in mouse and human systems: a comparative study. *Ann. N. Y. Acad. Sci.*, **1067**, 66–82.
65. Sandbach, J.M., Coscun, P.E., Grossniklaus, H.E., Kokoszka, J. E., Newman, N.J. and Wallace, D.C. (2001) Ocular pathology in mitochondrial superoxide dismutase (Sod2)-deficient mice. *Invest. Ophthalmol. Vis. Sci.*, **42**, 2173–2178.
66. Jakobs, T.C., Libby, R.T., Ben, Y., John, S.W. and Masland, R.H. (2005) Retinal ganglion cell degeneration is topological but not cell type specific in DBA/2J mice. *J. Cell. Biol.*, **171**, 313–325.
67. Soto, I., Pease, M.E., Son, J.L., Shi, X., Quigley, H.A. and Marsh-Armstrong, N. (2011) Retinal ganglion cell loss in a rat ocular hypertension model is sectorial and involves early optic nerve axon loss. *Invest. Ophthalmol. Vis. Sci.*, **52**, 434–441.
68. Chen, H., Wei, X., Cho, K.S., Chen, G., Sappington, R., Calkins, D.J. and Chen, D.F. (2011) Optic neuropathy due to microbead-induced elevated intraocular pressure in the mouse. *Invest. Ophthalmol. Vis. Sci.*, **52**, 36–44.
69. Chavez, J., Cano, C., Souki, A., Bermudez, V., Medina, M., Ciszek, A., Amell, A., Vargas, M.E., Reyna, N., Toledo, A. *et al.* (2007) Effect of cigarette smoking on the oxidant/antioxidant balance in healthy subjects. *Am. J. Ther.*, **14**, 189–193.
70. Zanon-Moreno, V., Garcia-Medina, J.J., Zanon-Viguer, V., Moreno-Nadal, M.A. and Pinazo-Duran, M.D. (2009) Smoking, an additional risk factor in elder women with primary open-angle glaucoma. *Mol. Vis.*, **15**, 2953–2959.
71. Lee, D., Shim, M.S., Kim, K.Y., Noh, Y.H., Kim, H., Kim, S.Y., Weinreb, R.N. and Ju, W.K. (2014) Coenzyme Q10 inhibits glutamate excitotoxicity and oxidative stress-mediated mitochondrial alteration in a mouse model of glaucoma. *Invest. Ophthalmol. Vis. Sci.*, **55**, 993–1005.
72. Payne, A.J., Kaja, S., Naumchuk, Y., Kunjukunju, N. and Koulen, P. (2014) Antioxidant drug therapy approaches for neuroprotection in chronic diseases of the retina. *Int. J. Mol. Sci.*, **15**, 1865–1886.
73. Yue, Y.K., Mo, B., Zhao, J., Yu, Y.J., Liu, L., Yue, C.L. and Liu, W. (2014) Neuroprotective effect of curcumin against oxidative damage in BV-2 microglia and high intraocular pressure animal model. *J. Ocul. Pharmacol. Ther.*, **30**, 657–664.
74. Joe, M.K., Kwon, H.S., Cojocaru, R. and Tomarev, S.I. (2014) Myocilin regulates cell proliferation and survival. *J. Biol. Chem.*, **289**, 10155–10167.